Unveiling dark structures with accurate weak lensing

Herbonnet, R.T.L.; Herbonnet R.T.L.

1

Introduction

1.1 Our view of the Universe

Curiosity for the unknown has been an essential trait for humanity, propelling it forward to discover ever larger parts of the place we live in. A phenomenal change in perspective on the Universe has come about in roughly the last hundred years. With improved technology luminous nebulae were observed in the sky, which were later revealed to be extragalactic objects (Hubble 1926) and in fact are galaxies much like our own Milky Way. Later on, Hubble (1929) showed that these galaxies in the local Universe are actually moving apart *at a constant speed* H_0 (the *Hubble constant*) according to what is now known as Hubble's law. This expansion of the Universe affects its contents, and for a Universe filled with matter (and radiation), expansion reduces the temperature, so that the early Universe would be small and have extremely high temperatures. Theoretically, elementary particles in the super-heated early Universe would be locked together in equilibrium reactions until the temperature had fallen enough to break equilibrium. At a certain point in time, the decrease in temperature would bind protons and electrons together in neutrons and photons suddenly had an unimpeded path through the Universe. This sudden burst of photons happened around 13.4 billion years ago at a temperature of around 3000 K. This wave of primordial photons was observed, accidentally at first, as a remarkably homogeneous black body spectrum at 2.73 K and is known as the cosmic microwave background (CMB). The lower temperature is evidence for the cooling of the Universe as it expands. An intriguing property of the CMB is its extreme homogeneity, given the large variation in density observed in the local Universe. This discovery hinted at some unknown force of gravity. Fritz Zwicky already coined the term 'dark matter' to describe some source of gravity keeping galaxies with extremely high rotational velocities together in clusters of galaxies, as their combined visible mass was far too low (Zwicky 1937). Later, Vera Rubin found that the visible light in galaxies could not provide enough mass to sustain the high stellar velocities (Rubin et al. 1980). Both studies provided evidence for the presence of invisible mass or a incomplete understanding of gravity at cosmological scales. A Universe filled with mass should have galaxies falling towards each other due to their gravitational attraction. It was therefore a huge surprise, worthy of a Nobel prize in 2011, when two teams, who looked at the fluxes of type Ia supernovae, which have known luminosities (after calibration), found that the distances were incompatible with a Universe dominated by matter (Riess et al. 1998; Perlmutter et al. 1999). Instead, they discovered that the Universe is not just expanding, but that the expansion is happening at an accelerated pace. These observations form the basis for the hot Big Bang model of the Universe, in which everything expanded from a single super-heated point in space.

The evolution of the Universe can be remarkably well described by a relatively sim-

ple model, known as the ΛCDM model. Although this model can describe a plethora of cosmological observations, the caveat is the unknown physical origins of two of its parameters. The Λ in the ΛCDM model refers to the cosmological constant. This constant is an additional parameter in Einstein's field equations for general relativity, which causes space-time to undergo accelerated expansion. A possible explanation in the framework of the standard model of particle physics is the energy of vacuum originating from the creation and annihilation of particles and their anti-particles. However, the predicted energy density of vacuum is off by many orders to explain the observed acceleration. Instead, the origin of the observed accelerated expansion of the Universe is being called *dark energy*, which could be the cosmological constant, or some other form of energy providing negative pressure on cosmological scales, and possibly evolving over time. The CDM in the ΛCDM model stands for cold dark matter. The mysterious gravitational force, seen by Zwicky and Rubin, is explained in the ΛCDM model by a form of matter, which does not interact through the electromagnetic force and has a temperature which is low enough so that it can cluster in large quantities, hence named cold dark matter. The abundance of atomic elements is precisely predicted by the Big Bang Nucleosynthesis and rule out any possible origin of dark matter as being a known particle, so a physical explanation is still missing. The remaining components of the Universe in the ΛCDM model are baryonic matter, radiation and the curvature of the Universe. The relative abundances of the components are ~70% dark energy, ~25% dark matter and only ~5% baryonic matter. The current abundance of radiation is tightly set by measurements of the CMB to be negligible. A period of rapid expansion in the first second of the Universe, known as inflation, which can explain, amongst other observables, the smooth distribution of matter in the CMB, predicts a Universe with very little curvature, consistent with, for instance, CMB measurements (Planck Collaboration et al. 2016a).

The dark, not well understood components of the ΛCDM model are also the dominant components of the Universe. The nature of dark matter and dark energy are some of the biggest open questions in cosmology and astrophysics. Precise measurements of the abundances of dark matter and dark energy would allow for tests of theoretical models. Currently, some of the tightest constraints come from measurements of the CMB. However, the CMB is one snapshot of the matter distribution in the very early Universe and dark energy is an effect which has only recently become dominant. Measuring the matter distributions at different epochs can put even tighter constraints on cosmological parameters and help to unravel the origins of dark matter and dark energy.

1.2 Structure in the Universe

Matter is not distributed uniformly throughout the Universe, instead there is large spatial variation. Local variation is apparent - the Earth is an overdensity of matter in its immediate surroundings - and on much larger scales stars and their planets are mainly contained in galaxies. But there is also structure on the largest scales. Galaxies tend to cluster together in groups and there is a large variety of environments. The bottom right panel of Figure 1.1 shows observations of galaxy positions. Galaxies are preferentially clustered along thin filaments, and the knots connecting the filaments contain many tens of galaxies, and in between there are large regions devoid of galaxies. This pattern is similar to the strands in a spider's web, and hence, the distribution of galaxies in the Universe is known as the Cosmic Web.

As mentioned before, from a cosmological perspective, the observable structure in the Universe posed a problem. The CMB shows a Universe where luminous matter was distributed very uniformly across the sky. Any gravitational collapse in the photon-baryon plasma would be washed out by Coulomb interactions and Compton scattering. The highest density regions seen in the CMB are overdense by only one part in one hundred thousand. In the time since the release of the CMB these regions could not have collapsed gravitationally under their own mass to form the myriad of high density structures seen today. The key to understanding structure formation is dark matter. Unlike the baryons-photon plasma, dark matter in the early Universe could already aggregate gravitationally into overdense regions. After the emission of the CMB, when baryons were free from the stifling interactions with photons, baryons fell into the dark matter potential wells. The early collapse of dark matter facilitated the growth of cosmological baryonic structures.

In Figure 1.1 snapshots of a numerical dark matter simulation at different redshifts are shown. The final snapshot (in the bottom left panel) shows a distribution of dark matter very similar to the Cosmic Web of galaxies. These dark matter structures grow in mass through gravitational accretion of material and mergers with other structures. Structures thus form hierarchically, such that small structures form first and the largest structures of the scale of galaxy clusters arise later. This history of mergers creates two classes of galaxies: *centrals* and *satellites*. Satellite galaxies were part of distinct structures which have merged with a larger structure. As a satellite galaxy falls into a cluster, it is stripped of its reservoirs of cool gas by tidal interactions and collision with the hot cluster gas. The deficiency of the cool gas hampers the ability of satellite galaxies to form new stars, leaving them with relatively old populations of stars, which give them a tell-tale reddish colour. On the other hand centrals reside in the centres of dark matter halos and have undergone different violent events. Through gravitational attraction they accrete material, growing in size and mass by cannibalising other galaxies. Violence is also suffered by the infalling halos around satellite galaxies, which are absorbed as a subhalo in the host halo. Numerical simulations suggest that during infall, subhaloes are stripped of dark matter by dynamical friction and tidal stripping (e.g. van den Bosch et al. 2016; Moliné et al. 2017). Measurements of the fate of infalling satellites can thus provide valuable information on the validity of the ΛCDM model.

Theoretical simulations of structure formation have also shown that the distribution of matter is very dependent on cosmology. Intuitively, this is to be expected. The growth of overdensities depends on the abundance of matter and is hampered by the (accelerated) expansion of the Universe. In addition, the growth is naturally dependent on the initial conditions of the density fluctuations. The initial state of fluctuations in the ΛCDM model is assumed to be isotropic and its power spectrum is described by a power law. The cosmological parameters for this power law are the slope n_s and an amplitude set by σ_8: the root mean square amplitude of matter fluctuations within a sphere of radius 8 Mpc. Computing the growth of structures from these initial conditions, numerical simulations can predict the abundance of large scale structure for any given cosmology. Measurements of the abundance of large scale structure at different epochs can be compared to these simulations to constrain cosmological parameters. Experiments have put constraints on Ω_m and σ_8, by measuring the abundance of the whole of large scale structure (Heymans et al. 2013; Kilbinger 2015; Jarvis et al. 2016) and the abundance of the largest structures (Henry 2004; Vikhlinin et al. 2009; Planck Collaboration et al. 2016b).

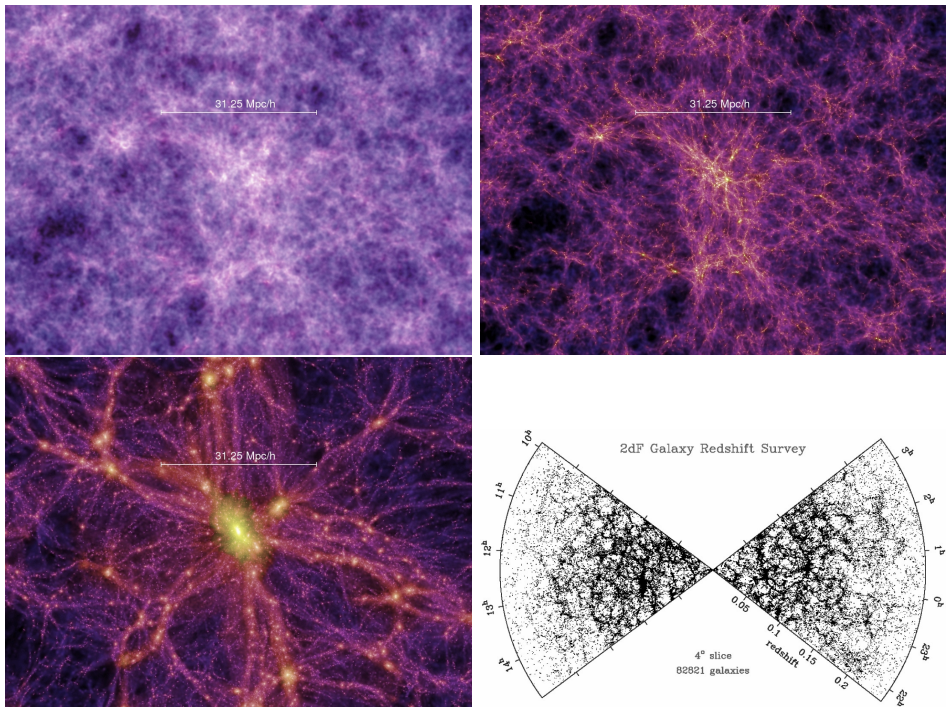

Figure 1.1: *Top left*: Snapshot at $z = 18.3$ of the distribution of cold dark matter particles in the Millennium simulation (Springel et al. 2005). *Top right*: Same area evolved to a redshift $z = 5.7$. *Bottom left*: Same area evolved to a redshift $z = 0$, showing a large variety of densities and strings of matter connecting the highest density (yellow) regions. *Bottom right*: Positions of real galaxies in the 2 Degree Field galaxy redshift survey (Peacock 2002). Due the filamentary structure the distribution of galaxies is refered to as the Cosmic Web. The similar distribution of galaxies and dark matter is due to the early agglomeration of dark matter and baryons falling into the dark matter overdensities.

Dark matter makes up the majority of mass in the Universe and any experiments of structure formation must necessarily include measurements of dark matter halos. Baryons trace the dark matter potential, so baryonic observables can be used to probe dark matter distributions. For instance, in galaxy clusters the density and temperature of the hot gas or the velocities of member galaxies can be used to obtain a mass estimate for the clusters. However, these estimates rely on simplifying assumptions of hydrostatic or dynamical equilibrium, which cannot be guaranteed given the turbulent formation history of clusters. Moreover, the whole scala of baryonic physics is currently not fully understood and instead, a more direct estimator of dark matter distributions is needed to calibrate baryonic observables.

1.3 Gravitational lensing

The study of dark matter requires looking at the only (known) force through which dark matter interacts: gravity. Almost exactly one hundred years ago Albert Einstein postulated the theory of general relativity, which describes gravity as the curvature in space-time around a massive object. A light ray always follows a straight path through space-time, but as it passes through a curved space-time, its trajectory will change. Because of the analogy to optical lenses, this effect is known as gravitational lensing, where the massive object serves as the *gravitational lens* or *lens* for short.

The distortion of the path of light from a background source depends on the curvature of space time and the distances between source and lens, source and observer, and lens and observer. Usually the distances between source, lens and observer are much larger than the extent of the lens, so that the lens can be approximated as a thin plane in which light rays are instantaneously deflected. Figure 1.2 shows a sketch of such a configuration for a point mass lens. The figure is taken from Bartelmann & Schneider (2001), the standard text known to probably everyone who studies gravitational lensing, and here I will briefly discuss the basics of gravitational lensing and I refer to that text for more details. In Figure 1.2, a light ray emitted by a source at coordinate $\boldsymbol{\beta}$ is observed at a location $\boldsymbol{\theta}$ instead, due to the deflection at the lens plane. The deflection angle $\boldsymbol{\alpha}$ depends on the mass of the lens M and the impact parameter ξ via

$$\hat{\boldsymbol{\alpha}} = \frac{4GM}{c^2\boldsymbol{\xi}}, \tag{1.1}$$

where c is the speed of light in vacuum and G the Newtonian gravitational constant. As can be seen from the figure, the deflection angle itself is not measurable, instead we look at the angle $\boldsymbol{\beta}$ which is tied to the deflection angle according to the *lens equation*:

$$\boldsymbol{\beta} = \boldsymbol{\theta} - \boldsymbol{\alpha}(\boldsymbol{\theta}), \tag{1.2}$$

where $\boldsymbol{\theta} = \boldsymbol{\xi}/D_\mathrm{d}$ and $\boldsymbol{\alpha} = \hat{\boldsymbol{\alpha}} D_\mathrm{ds}/D_\mathrm{d}$. Here $D_\mathrm{ds}, D_\mathrm{d}, D_\mathrm{s}$ are the anguler diameter distances between lens and source, observer and lens and observer and source, respectively, which can be obtained from the redshifts of lens and source. Equation 1.1 highlights the potential of gravitational lensing: a measurement of the deflection angle results in a mass estimate. However, the caveat is that gravitational lensing measures the projected 2D surface mass density along the line of sight $\Sigma(\boldsymbol{\xi})$, not the 3D mass distribution.

Gravitational lensing is produced by any massive lens with a bright background source. For example, evidence for Einstein's theory of general relativity was provided by Sir Arthur Eddington who looked at the displacement of stars behind the eclipsed

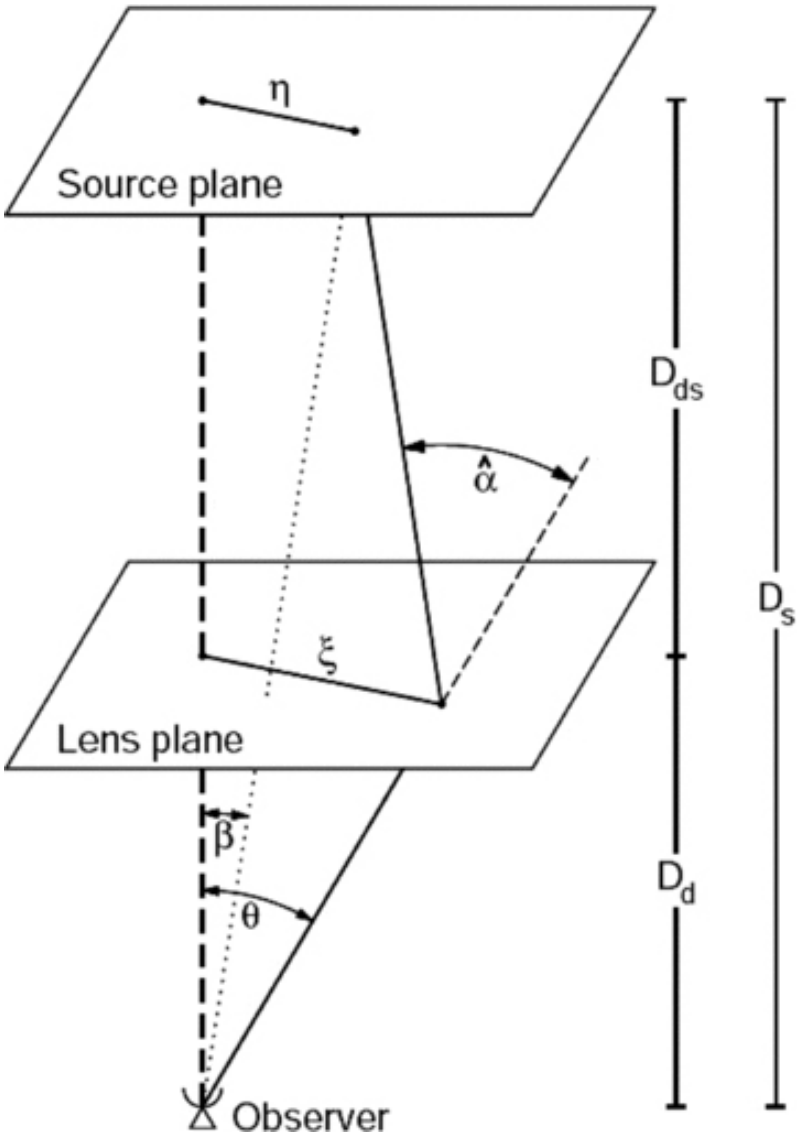

Figure 1.2: Graphical representation of the path of a light ray (shown as the solid line) from its source past a gravitational lens at the lens plane to the observer. The dashed line shows the direct line-of-sight between observer and source at location $\boldsymbol{\beta}$, whereas the object is also observed at the position $\boldsymbol{\theta}$. The deflection angle $\boldsymbol{\alpha}$, and hence the alternate postion $\boldsymbol{\theta}$, depends on the curvature induced by the massive lens and the distances between between the source, lens and/or observer. These distances are usually so much larger than the extent of the curved space-time that the lens can be approximated by a single plane. Original figure in (Bartelmann & Schneider 2001).

sun in 1919. The subject of this thesis is gravitational lensing by the largest structures in the Universe, for which the light sources are distant galaxies. Galaxies are extended objects, so that the simple sketch in Figure 1.2 has to be expanded for multiple light rays. For an observed galaxy, the light profile can be described by

$$I(\boldsymbol{\theta}) = \hat{I}(\boldsymbol{\beta}(\boldsymbol{\theta})) = \hat{I}(\boldsymbol{\beta}(\boldsymbol{\theta_0}) + \mathbf{A}(\boldsymbol{\theta_0})[\boldsymbol{\theta} - \boldsymbol{\theta_0}]), \tag{1.3}$$

where $I(\boldsymbol{\theta})$ gives the observed light intensity at angular position $\boldsymbol{\theta}$ and $\hat{I}(\boldsymbol{\beta}(\boldsymbol{\theta}))$ gives the light intensity at the source plane. As gravitational lensing conserves surface brightness, the two are equal. For the equation on the right hand side, we Taylor-expand the lens equation to first order around the location $\boldsymbol{\theta_0}$, assuming that the source is much smaller than the scales on which the lensing changes, which should be valid for large distances between observer, lens and source. The matrix $\mathbf{A}$ is given by

$$\mathbf{A}(\boldsymbol{\theta_0}) = \left.\frac{\partial \boldsymbol{\beta}}{\partial \boldsymbol{\theta}}\right|_{\boldsymbol{\theta_0}} = \delta_{ij} - \frac{\partial^2 \phi}{\partial \theta_i \partial \theta_j} = \begin{pmatrix} 1-\kappa-\gamma_1 & -\gamma_2 \\ -\gamma_2 & 1-\kappa+\gamma_1 \end{pmatrix}. \tag{1.4}$$

The lensing potential ϕ is related to the surface mass density via Poisson's equation $\nabla^2\phi(\boldsymbol{\theta}) = 2\kappa = \Sigma(\boldsymbol{\xi})/\Sigma_{\rm crit}$, where κ is known as the *convergence* and the critical surface mass density is a geometrical factor defined as

$$\Sigma_{\rm crit} = \frac{c^2}{4\pi G}\frac{D_{\rm s}}{D_{\rm ds} D_{\rm d}}. \tag{1.5}$$

In Equation 1.4 we have also defined the complex *shear* γ which is related to the lensing potential via

$$\gamma = \gamma_1 + i\gamma_2 = \frac{1}{2}\left(\frac{\partial^2\phi}{\partial\theta_1^2} - \frac{\partial^2\phi}{\partial\theta_2^2}\right) + i\frac{\partial^2\phi}{\partial\theta_1\partial\theta_2}. \tag{1.6}$$

The effect of gravitational lensing on an image of a background galaxy is to magnify the image and the tidal gravitational field stretches the galaxy's observed shape. Magnification has been used to search for the most distant galaxies in the early Universe (e.g. Zitrin et al. 2014). The gravitational shear induced by a lens can be visually appreciated as spectacular luminous arcs seen in massive galaxy clusters. These examples occur only rarely when a bright background object is directly on the line of sight of a very massive matter overdensity. A more frequent form of gravitational lensing occurs when the source galaxies are not directly in the line of sight and their images are only slightly distorted. This regime is known as weak lensing and is the main subject of this thesis. The common occurence of weak lensing makes it a powerful tool for observational cosmology, which is reflected in the large number of ongoing and upcoming weak lensing experiments. Surveys, such as the Kilo Degree Survey (de Jong et al. 2013), the Dark Energy Survey (The Dark Energy Survey Collaboration 2005), and the Hyper Suprime Cam survey (Miyazaki et al. 2012), are currently observing over thousand square degrees of the sky and in the future hemisphere-sized observations are planned with the *Euclid* satellite mission (Laureijs et al. 2011), the Large Synoptic Survey Telescope (Ivezic et al. 2008), and the Wide Field InfraRed Survey Telescope (Spergel et al. 2015). All these surveys will perform a cosmic shear analysis: a measurement of the shear-shear correlations between galaxies, which is a tracer for the distribution of dark matter structures. Comparison with theoretical cosmological models can provide constraints on the cosmological parameters governing the abundance and clustering of matter (see Kilbinger 2015 for a review). A tomographic analysis, in which galaxies

are divided into redshift bins, can also probe the time evolution of large scale structure and hence elucidate on dark energy. Tomographic cosmic shear has been hailed as one of the most powerful techniques for precise cosmological measurements.

1.4 Shape measurements

Weak gravitational lensing introduces small distortions in the observed shapes of distant galaxies, so the measurements of galaxy shapes are integral to weak lensing experiments. Projected light intensity profiles of galaxies can be very irregular and no single traditional shape can describe all galaxies, but we can generally consider galaxies as ellipses on the sky. The shape of an ellipse is fully described by a ratio between the semi-minor- and semi-major axes and the position angle, or equivalently by the two components of the ellipticity. The shear is a dimensionless spin-2 quantity, as is the ellipticity, so the ellipticity provides a natural observable for weak lensing. A galaxy with an intrinsic ellipticity will be observed after being gravitationally lensed to have an ellipticity (Seitz & Schneider 1997; Bartelmann & Schneider 2001)

$$\epsilon = \frac{\epsilon_\mathrm{s} + g}{1 + g^* \epsilon_s} \qquad \text{for } |g| \leq 1 \tag{1.7}$$

and

$$\chi = \frac{\chi_\mathrm{s} + 2g + g^2 \chi_\mathrm{s}^*}{1 + |g|^2 + 2\mathrm{Re}\left[g\chi_\mathrm{s}^*\right]}, \tag{1.8}$$

where ϵ and χ are the third flattening and third eccentricity, respectively. For an ellipse, these two definitions would be

$$\epsilon = \frac{1-q}{1+q} \mathrm{e}^{2i\zeta} \tag{1.9}$$

and

$$\chi = \frac{1-q^2}{1+q^2} \mathrm{e}^{2i\zeta} \tag{1.10}$$

for an axis ratio q and a position angle ζ. The subscript s for both definitions denotes the intrinsic shape of the galaxy at the source plane before it was sheared and an asterisk denotes a complex conjugate. The reduced shear g is the quantity measured in practice and it is related to the shear and convergence via $g = (1-\gamma)/\kappa$.

The shape of a galaxy can be computed from the second order moments of the galaxy surface brightness:

$$\epsilon = \frac{Q_{20} - Q_{02} + 2iQ_{11}}{Q_{20} + Q_{02} + 2\sqrt{Q_{20}Q_{02} - Q_{11}^2}} \tag{1.11}$$

and

$$\chi = \frac{Q_{20} - Q_{02} + 2iQ_{11}}{Q_{20} + Q_{02}}. \tag{1.12}$$

Here the moments of image brightness are defined as

$$Q_{ij} = \int \mathrm{d}^2 x \, I(x,y) \, (x - x_\mathrm{c})^i (y - y_\mathrm{c})^j, \tag{1.13}$$

where x and y are coordinates in the pixel image and the moments are evaluated around the galaxy centroid (x_c, y_c). The centroid can be estimated by finding the location where the flux Q_{00} of the galaxy is maximal, which is found by locating the coordinate (x_c, y_c) such that the first order moments $Q_{10} = Q_{01} = 0$. The moments of the image brightness provide an comprehensive set of quantities in which the pixel information in $I(x, y)$ is compressed. Combining many different orders can recover the original galaxy profile, although for weak lensing, typically, only the first few orders of moments are used.

Hypothetically, if all galaxies were circular, any anisotropy in the shape would be due to gravitational lensing. Unfortunately, galaxies have intrinsic ellipticities, which are usually much larger than the shear in the weak regime of gravitational lensing. It is therefore impossible to estimate the shear from a single galaxy. But according to the cosmological principle, galaxies should not have a preferential orientation, and galaxies in an ensemble should be round on average. This asumption of random projected shapes breaks down if there are intrinsic alignments between galaxies (see Joachimi et al. 2015 for a review). Mathematically we can rewrite Equations 1.7 and 1.8 for an ensemble average, assuming a small reduced shear $g \ll 1$ appropriate for weak lensing, to

$$\langle \epsilon \rangle \approx \langle \epsilon_s \rangle + g \approx g \tag{1.14}$$

and

$$\langle \chi \rangle \approx \langle \chi_s \rangle + 2g \approx 2g. \tag{1.15}$$

Here we assume that the intrinsic source ellipticities average to zero, so that the average observed value is a direct estimator of the gravitational reduced shear. The precision of a measurement of the shear is thus given by the number of galaxies in the ensemble. For ongoing cosmic shear surveys the precision is around a percent level, whereas future missions will have a precision of approximately one part-per-thousand.

The accuracy with which the shape of a galaxy can be measured directly affects the accuracy of the shear measurement. Although the task of measuring a shape sounds trivial, it is complicated by additional distortions to a galaxy's shape other than the gravitational shear. The excellent precision of upcoming cosmic shear surveys also puts unprecedented requirements on the accuracy of shape measurement methods. Here I review some of the main issues affecting accurate shape measurements on an image of a galaxy, although the full array of errors sources is much larger.

The effects undergone by light emitted from a distant galaxy are schematically shown in Figure 1.3 in chronological order from left to right. The leftmost panel shows the intrinsic light profile of some distant galaxy, which is sheared by gravitational lensing in the second panel. The shape of a galaxy becomes blurred as light rays travel through a turbulent atmosphere and telescope optics, which can be mathematically represented by a convolution with a point spread function (PSF). The PSF will have some shape, which is not identical to the shape of the sheared galaxy, so the convolution alters the observed shape. Although the middle panel sketches PSF convolution as a benign effect, the shape of a galaxy can be severely affected by the shape of the PSF, especially if the galaxy is small compared to the PSF. As weak lensing targets galaxies behind matter overdensities, source galaxies are often distant and thus small. The issue of the PSF is one of the main limitations in the recovery of accurate shapes and therefore, to remove the atmospheric contribution to the PSF, one of the future weak lensing experiments will be operated from a satellite. Next, the light rays hit the CCD cameras, which pixelises the galaxy image (fourth panel from the left in

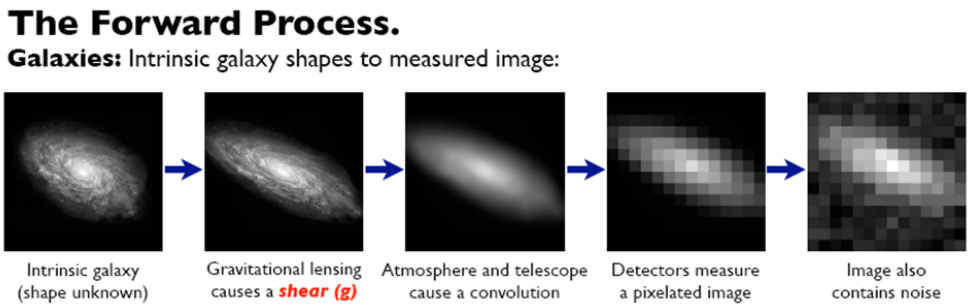

Figure 1.3: Sketch of the difficulties in shape measurement process. From left to right, the different processes affecting the light from a distant galaxy is shown in each panel, as the light rays move forward. Note that for visual effect the gravitational shear in the second panel is exaggerated by a factor ~ 10 to what is typical for weak gravitationally lensed galaxies. Original figure in (Bridle et al. 2009).

Figure 1.3). Pixelisation becomes troublesome for galaxies similar in size to the pixel scale. However, pixels are usually much smaller than the size of the PSF, and hence this issue has not received much attention. Finally, as is sketched for a very high signal-to-noise case in the rightmost panel, there is noise on the observed image from stray light, read out electronics, sky background and Poisson noise due to the finite amount of photons hitting the detector. Noise introduces an uncertainty in the observed light profile and this in turn introduces a bias in the measured shape of the galaxy: as can be seen from Equations 1.11 and 1.12 the ellipticity of a galaxy is a ratio of the observed light profile, and this non-linear dependence on the noisy data introduces a bias. Furthermore, the centroid is also measured from noisy data and as it appears non-linearly in Equation 1.13, it also adds to the *noise bias*.

1.4.1 Shape measurement techniques

A large amount of effort has been expended to find a method that can reliably measure galaxy shapes in the presence of observational nuisances. Early efforts (e.g. Kaiser et al. 1995) focused on using the moments of image brightness to estimate the ellipticity and are called *moment based methods*. The moments are measured with a weight function W which surpresses the noise at large distances from the galaxy centroid, which would otherwise dominate the integral

$$Q_{ij}^{w} = \int \mathrm{d}^2x\, I^{\mathrm{blur}}(x,y)\, W(x-x_\mathrm{c}, y-y_\mathrm{c})\, (x-x_\mathrm{c})^i (y-y_\mathrm{c})^j. \tag{1.16}$$

The choice of the weight function is arbitrary, as long as it reduces the effect of noise on large scales. The optimal choice would be the PSF convolved galaxy image I^{blur}, but as it is not available in practice, a Gaussian is a usual choice. The use of a weight function biases the ellipticity measurement, because Equations 1.7 and 1.8 are no longer formally correct. In addition, the galaxy image has been convolved by the PSF

$$I^{\mathrm{blur}}(x,y) = \int \mathrm{d}^2x\, I(x',y')\, P(x-x', y-y') \tag{1.17}$$

and the galaxy image has to be deconvolved. The PSF profile $P(x,y)$ can be obtained in practice by using stars in the observations as point sources on the sky which are

only affected by the atmosphere and telescope optics. The KSB method (Kaiser et al. 1995; Luppino & Kaiser 1997; Hoekstra et al. 1998) uses higher order (than two) moments to correct the observed third eccentricity χ for the use of the weight function and approximates the deconvolution using simplifying assumptions of the shape of the PSF. Later versions of moment-based methods have improved the algorithm by using elliptical weight functions matched to the shape of the galaxy and more accurate deconvolutions of the PSF profile (Melchior et al. 2011; Okura & Futamase 2011).

The approximate PSF deconvolution in early shape measurement methods could be overcome by forward modelling the galaxy image. In this approach, a model galaxy is generated and convolved with the PSF model. This convolved galaxy model is then fit to the observed galaxy by adjusting its properties, such as size, flux and ellipticity. The intrinsic ellipticity of the best fit galaxy model can then be used to estimate the shear. For obvious reason, this class of methods is refered to as *model fitting methods* in the literature, and two distinct galaxy models have been used: a linear combination of *shapelets* (e.g. Refregier & Bacon 2003; Massey & Refregier 2005; Kuijken 2006) and a linear combination of parametric profiles (e.g. Kuijken 1999; Miller et al. 2007; Zuntz et al. 2013; Jarvis et al. 2016). Shapelets are a set of basis functions which can describe a plethora of astronomical objects and have a well defined convolution operator. The downside of shapelets, and the reason that shapelet-based methods are not employed in ongoing large weak lensing experiments, is that the number of shapelets needs to be truncated because higher orders are more prone to noise, and the truncation leads to a biased shape measurement. Alternatively, parametric profiles provide a simpler fitting model. Sérsic profiles (Sérsic 1963) are a family of parametric radial profiles of the form $\ln\left[I(x,y)\right] \sim -(x^2+y^2)^{1/2n}$ often used to describe galaxy light profiles. Some descriptions of galaxies used in the literature are linear combinations of Gaussians ($n = 0.5$) or the sum of an exponential disk ($n = 1$) and a De Vaucouleurs bulge ($n = 4$). Although the PSF convolution is accurately handled by this type of shape measurement method, a large assumption is made on the light profile of galaxies. The potential danger of using Sérsic profiles is that they might not capture the full morphological complexity of real galaxies, leading to a possible *model bias* in the ellipticity estimate (Voigt & Bridle 2010; Bernstein 2010).

Recently, the weak lensing community has focused more on noise bias and several new methods have been developed to reduce the effect. Noise bias is caused by a non-linear dependence of the shear estimator on the noisy image data (Hirata et al. 2004; Melchior & Viola 2012; Viola et al. 2014). For any method, noise is an addition to the galaxy image and is subject to the same mathemathical formalism. Some authors have used this to calculate the effect of noise on the resulting shear estimate and implicitly correct the estimate for noise bias with notable success (Refregier et al. 2012; Okura & Futamase 2013). Alternatively, Bernstein & Armstrong (2014) have developed a Bayesian method which circumvents noise bias by removing non-linear dependence on the noisy image and the method shows good promise for the future (Bernstein et al. 2016).

1.4.2 Image simulations

A quantitative statement on the performance of shape measurement methods is necessary before they can be reliably applied on data. Given the size and depth of the survey and the desired constraints on cosmological parameters, there is a maximum

allowed bias. The biases in a shape measurement method are generally expressed by

$$g_i^{\rm meas} = g_i^{\rm true}(1 + m_i) + c_i, \tag{1.18}$$

where m and c are the multiplicative and additive biases, respectively, in the measured shear $g_i^{\rm meas}$ compared to the true shear $g_i^{\rm true}$, for the two components of the shear. A multiplicative bias can arise due to noise or PSF convolution and an additive bias from any coherent sources of anisotropy, such as an imperfect correction of an elliptical PSF. Because the full process undergone by light rays is well understood, it can be simulated and these image simulations are currently the only reliable way to quantify the accuracy of shape measurement methods. Emulating telescope images will subject the method to the same difficulties faced in real observations, some of which can not be modelled otherwise, such as for instance the blending of the light of neighbouring galaxies, the impact of the detection algorithm, or stars misclassified as source galaxies.

The weak lensing community has a long history of community wide image simulations to improve overall understanding of systematic effects. The different performance of different implementations of the same method prompted the team behind the 'shear testing programme' (STEP; Heymans et al. 2006) to create large suites of simulated observations with known input shears. Different groups then ran their method on these simulated images to compute the shear, which when compared to the input shear gives the bias in their method. This exercise clearly showed that different choices could influence the performance. The first STEP was followed by a second programme (Massey et al. 2007) in which they searched for the perfect unbiased method. Instead, no unbiased method was found and the community turned to a new programme, which aimed to characterise the sources of bias inherent to methods. The 'gravitational lensing accuracy testing' (GREAT) challenges (Bridle et al. 2010; Kitching et al. 2012; Mandelbaum et al. 2015) were set up using much simpler image simulations to address individual sources of bias. These simulations contain only postage stamps of isolated galaxies and had different branches with different realistic complexities, such as constant versus varying shear profiles or parametric galaxy models versus actual galaxy images.

All of these public suites of image simulations have been of tremendous value to the weak lensing community. Each has pushed the understanding of sources of systematic error further and provides a benchmark on which to test new methods. The latest challenge has also provided the community with the well-tested software package `GalSim` with which to produce image simulations (Rowe et al. 2015). However, by systematically going through realistic features of telescope observations these simulations have shown the importance of having realistic image simulations with which to calibrate the observations. The input of the simulations has a strong effect on the bias measured from the simulations (Hoekstra et al. 2015; Kannawadi et al. 2015; Hoekstra et al. 2016) and realistic input is thus imperative for the calibration of shape measurement methods with image simulations. Different weak lensing experiments will have varying observational conditions, survey strategies and camera characteristics, which all affect the bias in the measurement. The requirement of percent level precision in the shear estimates posed by ongoing surveys already limits the use of general simulations for individual surveys. Instead, each cosmic shear survey requires its own dedicated set of image simulations (Miller et al. 2013; Jarvis et al. 2016).

1.5 This thesis

Weak gravitational lensing has the potential to provide excellent cosmological constraints from the evolution of large scale structure. However, the accuracy of weak lensing measurements is severely degraded because observational effects distort the shapes of galaxies, mimicking a shear signal. The first half of this thesis is concerned with these systematic sources of errors and how they can be mitigated.

In **Chapter 2** we develop a new shape measurement method which deals analytically with PSF convolution and noise in the image. We present the theoretical framework and test the method on simple image simulations to quantify the accuracy. We show that our method is capable of reaching subpercent accuracy even for small and noisy galaxies, which, taken at face value, is sufficient for ongoing cosmic shear surveys. However, more testing on more realistic image simulations is needed to characterise the performance for a whole host of observational effects.

At the beginning of 2016 the Kilo Degree Survey (KiDS) had observed roughly 450 square degrees of the sky. This provided us with the largest area to date for a cosmic shear analysis, but also put unprecedented requirements on the systematic uncertainties. **Chapter 3** describes the performance testing of the shape measurement algorithm used in the cosmic shear analysis. In this massive endeavour, I was responsible for the creation of a large suite of dedicated image simulations specifically designed to match the KiDS data as closely as possible. Some discrepancies between simulations and observations remained and so I performed extensive sensitivity analyses to ensure that the discrepancy did not affect the shear estimate beyond the precision afforded by the simulations. After all these tests we could confidently claim a residual multiplicative shear bias of 0.01 ± 0.01 and a negligibly small additive bias. This work has been an indispensible part of the analysis of the KiDS data and provided a calibration with enough precision for the KiDS cosmic shear analysis (Hildebrandt et al. 2017), and the calibration has since been used by every paper using the KiDS data.

The second half of this thesis focuses on weak lensing measurements using observations of galaxy clusters. For the analysis of Hoekstra et al. (2015), I created large suites of image simulations in an exercise similar to the GREAT challenges. We analysed simulations with ever increasing complexity to systematically account for various sources of error in the shear measurement pipeline, and eventually calibrated the algorithm for these biases. The increased accuracy of the shear estimates helped to obtain improved mass estimates for the sample of galaxy clusters studied in Hoekstra et al. (2015) compared to earlier work by Hoekstra et al. (2012). For this thesis I used this improved pipeline to study another large sample of clusters observed as part of the Multi Epoch Nearby Cluster Survey. Other factors affecting the accuracy of the weak lensing mass estimates are the determination of the critical surface density from the redshift distribution of source galaxies and the purity of the sample of source galaxies. I used auxiliary deep data containing reliable photometric redshift estimates to derive a source redshift distribution. With image simulations, similar to those used in **Chapter 3**, I studied the incompleteness of the population of background source galaxies due to obscuration by cluster members. Incorporating this incompleteness, I compute the purity of the source galaxy sample and statistically correct our weak lensing signal.

In **Chapter 4** we use our pipeline to measure the weak lensing masses of a large set of galaxy clusters. These total masses are combined with the sample of Hoekstra et al. (2015) and then used to determine a scaling relation with the mass estimate based on measurements of the hot cluster gas. We find that a mass dependent scaling relation is

favoured by our data over a constant bias in the gas-based mass measurements. Given the large statistical power of our full cluster sample, our findings may help to resolve the tension found between the cosmological parameters estimated from the primary CMB measurements and those estimated using the abundance of galaxy clusters.

In **Chapter 5** we apply our pipeline to the dark matter halos around satellite galaxies in the same sample of galaxy clusters. Shape measurements of galaxies are affected by light of nearby galaxies, which is a major concern in the crowded cluster environment. I calibrated the shape measurement algorithm for this effect with dedicated image simulations and determined the minimum radius from the galaxy centre for accurate weak lensing measurements. We constrain the relation between subhalo mass and stellar mass and find it to be consistent with expectations. There is no sign of significant mass segregation in our data, contrary to what has been found by other works.

Bibliography

Bartelmann M., Schneider P., 2001, Phys. Rep., 340, 291

Bernstein G. M., 2010, MNRAS, 406, 2793

Bernstein G. M., Armstrong R., 2014, MNRAS, 438, 1880

Bernstein G. M., Armstrong R., Krawiec C., March M. C., 2016, MNRAS, 459, 4467

Bridle S., et al., 2009, Annals of Applied Statistics, 3, 6

Bridle S., et al., 2010, MNRAS, 405, 2044

Henry J. P., 2004, ApJ, 609, 603

Heymans C., et al., 2006, MNRAS, 368, 1323

Heymans C., et al., 2013, MNRAS, 432, 2433

Hildebrandt H., et al., 2017, MNRAS, 465, 1454

Hirata C. M., et al., 2004, MNRAS, 353, 529

Hoekstra H., Franx M., Kuijken K., Squires G., 1998, ApJ, 504, 636

Hoekstra H., Mahdavi A., Babul A., Bildfell C., 2012, MNRAS, 427, 1298

Hoekstra H., Herbonnet R., Muzzin A., Babul A., Mahdavi A., Viola M., Cacciato M., 2015, MNRAS, 449, 685

Hoekstra H., Viola M., Herbonnet R., 2016, preprint, (`arXiv:1609.03281`)

Hubble E. P., 1926, ApJ, 64

Hubble E., 1929, Proceedings of the National Academy of Science, 15, 168

Ivezic Z., et al., 2008, preprint, (`arXiv:0805.2366`)

Jarvis M., et al., 2016, MNRAS, 460, 2245

Joachimi B., et al., 2015, Space Sci. Rev., 193, 1

Kaiser N., Squires G., Broadhurst T., 1995, ApJ, 449, 460

Kannawadi A., Mandelbaum R., Lackner C., 2015, MNRAS, 449, 3597

Kilbinger M., 2015, Reports on Progress in Physics, 78, 086901

Kitching T. D., et al., 2012, MNRAS, 423, 3163

Kuijken K., 1999, A&A, 352, 355

Kuijken K., 2006, A&A, 456, 827

Laureijs R., et al., 2011, preprint, (`arXiv:1110.3193`)

Luppino G. A., Kaiser N., 1997, ApJ, 475, 20

Mandelbaum R., et al., 2015, MNRAS, 450, 2963

Massey R., Refregier A., 2005, MNRAS, 363, 197

Massey R., et al., 2007, MNRAS, 376, 13

Melchior P., Viola M., 2012, MNRAS, 424, 2757

Melchior P., Viola M., Schäfer B. M., Bartelmann M., 2011, MNRAS, 412, 1552

Miller L., Kitching T. D., Heymans C., Heavens A. F., van Waerbeke L., 2007, MNRAS, 382, 315

Miller L., et al., 2013, MNRAS, 429, 2858

Miyazaki S., et al., 2012, in Ground-based and Airborne Instrumentation for Astronomy IV. p. 84460Z, doi:10.1117/12.926844

Moliné Á., Sánchez-Conde M. A., Palomares-Ruiz S., Prada F., 2017, MNRAS, 466, 4974

Okura Y., Futamase T., 2011, ApJ, 730, 9

Okura Y., Futamase T., 2013, ApJ, 771, 37

Peacock J. A., 2002, in Metcalfe N., Shanks T., eds, Astronomical Society of the Pacific Conference Series Vol. 283, A New Era in Cosmology. p. 19 (`arXiv:astro-ph/0204239`)

Perlmutter S., et al., 1999, ApJ, 517, 565

Planck Collaboration et al., 2016a, A&A, 594, A13

Planck Collaboration et al., 2016b, A&A, 594, A24

Refregier A., Bacon D., 2003, MNRAS, 338, 48

Refregier A., Kacprzak T., Amara A., Bridle S., Rowe B., 2012, MNRAS, 425, 1951

Riess A. G., et al., 1998, AJ, 116, 1009

Rowe B. T. P., et al., 2015, Astronomy and Computing, 10, 121

Rubin V. C., Ford Jr. W. K., Thonnard N., 1980, ApJ, 238, 471

Seitz C., Schneider P., 1997, A&A, 318, 687

Sérsic J. L., 1963, Boletin de la Asociacion Argentina de Astronomia La Plata Argentina, 6, 41

Spergel D., et al., 2015, preprint, (arXiv:1503.03757)

Springel V., et al., 2005, Nature, 435, 629

The Dark Energy Survey Collaboration 2005, ArXiv Astrophysics e-prints,

Vikhlinin A., et al., 2009, ApJ, 692, 1060

Viola M., Kitching T. D., Joachimi B., 2014, MNRAS, 439, 1909

Voigt L. M., Bridle S. L., 2010, MNRAS, 404, 458

Zitrin A., et al., 2014, ApJL, 793, L12

Zuntz J., Kacprzak T., Voigt L., Hirsch M., Rowe B., Bridle S., 2013, MNRAS, 434, 1604

Zwicky F., 1937, ApJ, 86, 217

de Jong J. T. A., Verdoes Kleijn G. A., Kuijken K. H., Valentijn E. A., 2013, Experimental Astronomy, 35, 25

van den Bosch F. C., Jiang F., Campbell D., Behroozi P., 2016, MNRAS, 455, 158